Development of a New Type-I Isotherm for Correction of Langmuir Isotherm's Over-estimation of Adsorption at Higher Pressures

Adeolu J. Alawode[1*] and Olugbenga A. Falode[1]

[1]*Department of Petroleum Engineering, University of Ibadan, Ibadan, Nigeria.*

Authors' contribution

This work was carried out in collaboration between both authors. Authors AJA and OAF designed the study. Author AJA performed the statistical analysis and wrote the protocol and the first draft of the manuscript under the supervision of author OAF. Both authors managed the literature searches, the analyses of the study, read and approved the final manuscript.

Original Research Article

ABSTRACT

Different gas equilibrium adsorption models (or isotherms) with various theoretical frameworks have been applied to quantify adsorbed volume (V) of gas (or fluid) through pressure-volume behaviour at a constant temperature. Most often, Langmuir isotherm (representing Type I Isotherm) has been used in modelling monolayer adsorption even though it yields over-estimation at higher pressures thus contradicting the description of Type I isotherm. Here, higher pressures refer to pressures above the adsorption saturation pressure (P_s). Hence, in this work, a new Type I adsorption isotherm involving pressure(P), adsorption saturation pressure (P_s), maximum adsorbed volume (V_{max}) and adsorbate-adsorbent resistance parameter (n) was developed using kinetic approach. The developed adsorption isotherm is $V = \begin{cases} V_{max}\left\{\frac{P}{P_s} + \left(1 - \frac{P}{P_s}\right)\left(\frac{P}{P_s}\right)^n\right\}, for\ P < P_s \\ V_{max},\ for\ P \geq P_s \end{cases}$ and it

---

*Corresponding author: E-mail: adelawode@yahoo.com;

shows that V_{max} is attained when pressure increases to P_s, above which no further gas adsorption occurs. The developed isotherm can be used to model all cases of monolayer adsorptions of gases (or fluids) on adsorbents. The developed and Langmuir isotherms were used in modelling secondary low-pressure gas adsorption data of different adsorbents and the qualities of fit were statistically assessed. For laboratory methane adsorption on Turkey's shale sample at 25°C, the developed isotherm yields a correlation with an R^2 value of 0.997 and predicts a maximum adsorption volume of 0.0450 mmol g^{-1} at a P_s of 2,005 psia. However, Langmuir isotherm yields a correlation with an R^2 value of 0.989 and predicts a maximum adsorption volume (Langmuir volume, V_L) of 0.0548 mmol g^{-1} at infinite P_s. At the higher-pressure range, the developed isotherm reveals that Langmuir isotherm is not a Type I isotherm but a "*pseudo-Type I*" isotherm.

1. INTRODUCTION

Adsorption is the adhesion of molecules of a gas, liquid or dissolved solid to a surface to form a thin film of the adsorbate on the adsorbent. Adsorption can be classified as *physisorption* (physical adsorption) or *chemisorption* (chemical adsorption). A practical classification of particular adsorption as physisorption or chemisorption depends principally on the temperature-dependent binding energy of the adsorbate to the adsorbent. However, the same surface can display physisorption at one temperature and chemisorption at higher temperature [1].

Gas adsorption (or desorption) occurs when the interaction forces in the region of the phase boundary (i.e., solid surface) are altered. The interaction forces are in the form of (i) the van der Waals forces that cause physical attraction, (ii) electrostatic/ionic forces that cause surface charge interaction, (iii) covalent bonding that causes chemical attraction, and (iv) the adsorbent hydrophilic or hydrophobic nature.

Three major approaches that form the basis of formulating adsorption models or isotherms are kinetics, thermodynamics and potential theory [2]. Kinetic consideration is based on adsorption equilibrium which is defined as a state of dynamic equilibrium attained when an adsorbate containing phase has been in contact with the adsorbent for sufficient time, with both adsorption and desorption rates being equal [3,4,5].

Different models with various theoretical backgrounds have been applied to describe the adsorption behaviour of fluids. These models include linear adsorption isotherm, Freundlich adsorption isotherm [6], Langmuir adsorption isotherm [3], extended Langmuir adsorption isotherm [7], Brunauer-Emmett-Teller (BET) adsorption model [8], Fowler-Guggenheim adsorption isotherm [9], Temkin adsorption isotherm [10], Harkins-Jura adsorption isotherm [11], Langmuir-Freundlich (or Sips) adsorption isotherm [12], Koble–Corrigan adsorption isotherm [13], Kiselev adsorption isotherm [14], Redlich-Peterson adsorption isotherm [15], Elovich adsorption isotherm [16], ideal adsorbed solution (IAS) theory [17], Dubinin's micropores filling models [18,19,20,21], Toth adsorption isotherm [22], multisite occupancy model [23], etc.

The theory-based equilibrium physisorption models applicable to unconventional gas reservoirs are the Ono-Kondo (OK) lattice model, two-dimensional equations of state (2-D EOS) adsorption model (including Hill-de Boer adsorption isotherm) and simplified local density (SLD) models.

The experimentally observed adsorption isotherms are grouped according to the International Union of Pure and Applied Chemistry (IUPAC) recommendations [24] in six different types I to VI (Fig. 1).

Type I isotherms are characterized by the maximum value the mass adsorbed attains and maintains even at very high gas (or fluid) pressures. The model is applicable in microporous materials exhibiting monolayer adsorption. Type I isotherms are often described by the Langmuir equation. Type II isotherms describe typical adsorption in mesoporous materials exhibiting monolayer at low pressures and multilayer at higher pressures near saturation and pore condensation with no hysteresis. Type II isotherms often can be described by the BET equation [25].
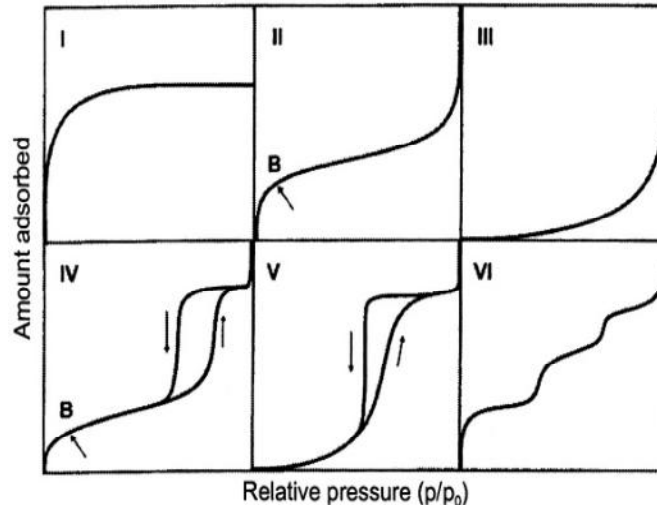
Fig. 1. Main types of gas physisorption Isotherms [24,26]

Type III isotherms occur in systems where the adsorbate-adsorbate interaction is stronger than the adsorbate-adsorbent interaction. Type IV isotherms describe the adsorption behaviour of special mesoporous materials showing pore condensation together with hysteresis behaviour between the adsorption and the desorption paths [25].

Type V isotherms (unlike the Type IV isotherms) features nearly perpendicular middle portions of the adsorption and the desorption paths often near relative gas pressures. This shows the existence of mesoporous in which phase change like pore condensation may occur. Type VI isotherms are characterized by stepwise multilayer adsorption; the layers becoming more pronounced at low temperatures [25].

Most often, Langmuir isotherm (representing Type I Isotherm) has been used in modelling gas adsorption in coal bed reservoirs, shale gas reservoirs and other monolayer adsorptions cases although it yields over-estimation at higher pressures thus contradicting the description of Type I isotherm. Here, higher pressures refer to pressures above the adsorption saturation pressure (P_s). Langmuir isotherm is used in modelling monolayer gas adsorption because of its ease of application and its reliable low-pressure adsorption prediction [27,28,29,30, 31,32,33].

Hence, in this work, a new Type-I adsorption isotherm (which assumes monolayer adsorption like Langmuir isotherm) is developed that discloses and amends this ambiguity.

2. METHODOLOGY

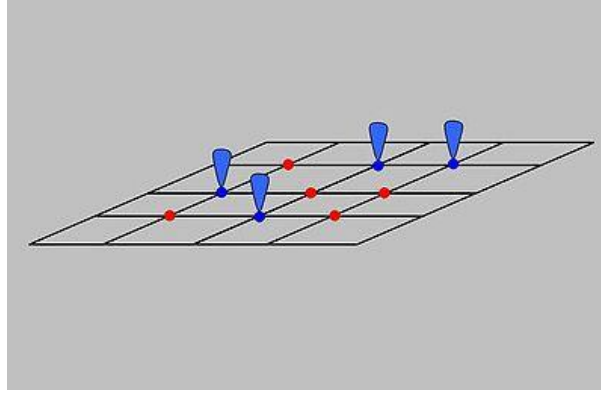### 2.1 Physical Depiction of Adsorption in the New Model

The physical depiction of adsorption of the molecules of a fluid F in the new model is shown in Fig. 2.

Here, the occupied surface sites are denoted as blue clips while vacant surface sites are denoted as red spots on the surface.

2.1.1 Assumptions

The basic assumptions made here are similar to those of the Langmuir isotherm. The model assumes an ideal surface where: (i) solid surface is composed of localised adsorption sites and each site can hold only one adsorbate molecule, (ii) adsorption sites are energetically equivalent i.e. the surface is homogeneous and all sites are identical, (iii) saturation coverage is attained when all sites are completely occupied, (iv) adsorption of molecules is of monolayer type and (v) adsorption is reversible i.e. desorption occurs during pressure depletion.

Additional (major) assumptions included are: (i) there are adsorbate-adsorbate interactions between neighbouring adsorption sites, (ii) attainment of a definite adsorption saturation pressure and (iii) dynamic equilibrium parameter K_{eq}^f is not considered constant (as done in Langmuir isotherm derivation where adsorption coverage is assumed to be independent of the

Fig. 2. Physical depiction (Schematic) of adsorption in the new model [3]

enthalpy of adsorption E) because adsorption coverage actually depends on the enthalpy of adsorption E (adsorption saturation pressure P_s is an index of adsorption coverage).

2.1.2 Development of the new adsorption model: Kinetic approach

In the adsorption of the molecules of a fluid F, the concentration of the occupied surface sites is denoted as $[S_{ads}]$ (number/area) while the vacant surface sites concentration is denoted as $[S_{vac}]$. Total site concentration is $[S_T] = [S_{ads}] + [S_{vac}]$ (number/area).

Rate of adsorption R_{ads} is proportional to the adsorption potential of the fluid (at pressure P) towards saturation coverage of the surface. The saturation coverage is, of course, attained when all sites $[S_T]$ (number/area) are completely occupied. Attractive interactions causing adsorption are characterized by adsorbates losing activation energy, thus adsorption is an exothermic reaction.

Consequently,

$$R_{ads} = \beta_{ads}.P.[S_T] \qquad (1)$$

Where adsorption rate parameter β_{ads} is expressed as an Arrhenius relation:

$$\beta_{ads} = K_{ads_o} \cdot exp\left(\frac{-E}{RT}\right) \qquad (2)$$

and K_{ads_o} is adsorption rate coefficient at the onset of adsorption, E is interaction energy (i.e., heat or enthalpy of adsorption) between the gas molecules and the solid sites, R is universal gas constant and T is temperature.

On the other hand, rate of desorption R_{des} is proportional to the difference between the desorption potential of the fluid (at the adsorption saturation pressure P_s) towards partial coverage of the surface $[S_{ads}]$, and the adsorption potential at a lower pressure P.

$$R_{des} = K_{des} \cdot \{P_s[S_{ads}] - P[S_T]\} \qquad (3)$$

Where K_{des} is desorption rate coefficient, P_s is the adsorption saturation pressure, the pressure at which adsorbed volume saturation is attained (as pressure increases) and the commencement of gas desorption (during pressure depletion).

The dynamic equilibrium parameter K_{eq}^f is expressed as:

$$K_{eq}^f = \frac{\beta_{ads}}{K_{des}} = \frac{K_{adso}}{K_{des}} \cdot exp\left(\frac{-E}{RT}\right) \qquad (4)$$

As stated earlier, K_{eq}^f is only constant if adsorption coverage is assumed to be independent of the enthalpy of adsorption E as done in Langmuir isotherm derivation. However, here, K_{eq}^f is not considered constant because adsorption coverage depends on the enthalpy of adsorption E (adsorption saturation pressure is an index of adsorption coverage).

At dynamic equilibrium, the rate of absorption equals the rate of desorption. Hence, the dynamic equilibrium parameter K_{eq}^f is expressed as:

$$K_{eq}^f = \frac{\beta_{ads}}{K_{des}} = \frac{\{P_s[S_{ads}] - P[S_T]\}}{P[S_T]} \qquad (5)$$

$$K_{eq}^f = \frac{P_s[S_{ads}]}{P[S_T]} - 1 \qquad (6)$$

$$\frac{P_s[S_{ads}]}{P[S_T]} = 1 + K_{eq}^f \tag{7}$$

$$\frac{[S_{ads}]}{[S_T]} = \frac{P\left(1+K_{eq}^f\right)}{P_s} \tag{8}$$

Expressing the occupied sites $[S_{ads}]$ as the adsorbed volume V at pressure P and the concentration of all sites $[S_T]$ as the maximum adsorbed volume V_{max} at and above the onset of adsorption saturation pressure i.e. $P \geq P_s$; then

$$\frac{V}{V_{max}} = \frac{P\left(1+K_{eq}^f\right)}{P_s} \tag{9}$$

Where K_{eq}^f is a measure of the pressure deviation from the corresponding linear isotherm pressure

$$V = V_{max}\left(\frac{P+K_{eq}^f P}{P_s}\right) \tag{10}$$

Expressing $K_{eq}^f P$ as P_a the pressure deviation from the corresponding linear isotherm pressure, then:

$$V = V_{max}\left(\frac{P}{P_s} + \frac{P_a}{P_s}\right) \tag{11}$$

1: For under-saturated adsorption, i.e. when $0 \leq P < P_s$

The pressure deviation from the corresponding linear isotherm pressure is proportional to pressure deviation from the adsorption saturated pressure:

$$P_a = k(P_s - P) \tag{12}$$

Where k is a dynamic parameter expressed as:

$$k = \left(\frac{P}{P_s}\right)^n \tag{13}$$

Where n is the adsorbate-adsorbent resistance parameter

Consequently,

$$P_a = (P_s - P)\left(\frac{P}{P_s}\right)^n \tag{14}$$

K_{eq}^f is further simplified as:

$$K_{eq}^f = \left(\frac{P}{P_s}\right)^{n-1} - \left(\frac{P}{P_s}\right)^n \tag{15}$$

This shows that the dynamic equilibrium parameter K_{eq}^f is a function of pressure P and

adsorption saturation pressure P_s: as P changes, K_{eq}^f also changes unlike the case in Langmuir isotherm derivation where K_{eq}^f is considered constant irrespective of the level of P.

It should be noted that when there is no adsorption, $P = 0$ and thus $P_a = 0$. Also, at the onset of adsorption saturation pressure $P = P_s$ and thus $P_a = 0$.

Substituting Equation 14 into Equation 11 gives:

$$V = V_{max}\left\{\frac{P}{P_s} + \left(1 - \frac{P}{P_s}\right)\left(\frac{P}{P_s}\right)^n\right\} \tag{16}$$

Where V is the adsorbed volume at pressure P, V_{max} is the maximum adsorbed volume at and above the saturation pressure, and n is adsorbate-adsorbent resistance parameter. The major representatives of Type I adsorption isotherm pressure-volume data (below the adsorption saturation pressure) are captured and depicted by the adsorbate-adsorbent resistance parameter n ranging from 0.30 to 1.15.

2: For saturated adsorption, i.e. when $P \geq P_s$

The adsorption saturated pressure P_s is the effective pressure while an additional increase in pressure is latent; hence, the heat of adsorption $E = 0$. Thus

$$V = V_{max} \tag{17}$$

2.2 Statement of the Developed Adsorption Isotherm

The developed adsorption isotherm is stated as follows:

$$V = \begin{cases} V_{max}\left\{\frac{P}{P_s} + \left(1 - \frac{P}{P_s}\right)\left(\frac{P}{P_s}\right)^n\right\}, for\ P < P_s \\ V_{max},\ for\ P \geq P_s \end{cases} \tag{18}$$

Where V is the adsorbed volume at equilibrium pressure P, P_s is the adsorption saturation pressure at which the maximum adsorbed volume V_{max} is attained, n is adsorbate-adsorbent resistance parameter (n ranges from 0.30 to 1.15).

2.3 Establishment of Boundary Conditions for the Developed Adsorption Isotherm

The graphical analysis of establishing boundary conditions for the developed adsorption isotherm is shown in Fig. 3.
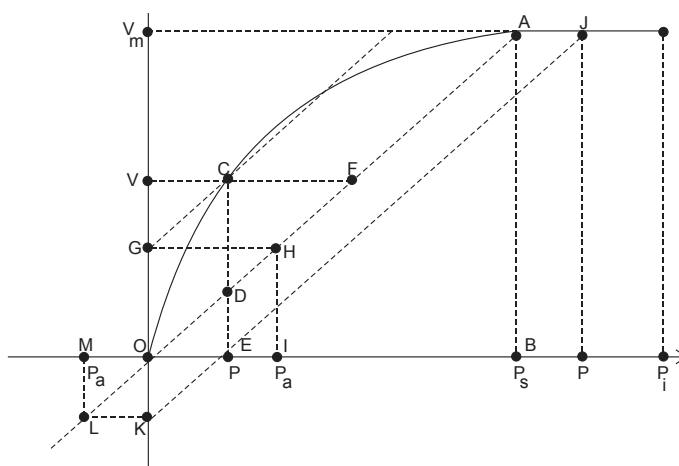
Fig. 3. Graphical analysis of the developed adsorption isotherm

For an adsorbed volume V, point C on the isotherm is projected downwards to meet line $\overline{OA}$ at D and the pressure axis at E. The volume deviation from the corresponding linear isotherm volume is $\overline{CD} = \delta$.

Along $\overline{OA}$,

$$slope = \frac{\overline{DE}}{\overline{OE}} = \frac{\overline{AB}}{\overline{OB}} \tag{19}$$

But

$$\overline{DE} = \overline{CE} - \overline{CD} \tag{20}$$

i.e.

$$\overline{DE} = V - \delta \tag{21}$$

Consequently,

$$slope = \frac{V - \delta}{P} = \frac{V_{max}}{P_s} \tag{22}$$

$$\frac{V - \delta}{V_{max}} = \frac{P}{P_s} \tag{23}$$

$$\frac{V}{V_{max}} = \frac{P}{P_s} + \frac{\delta}{V_{max}} \tag{24}$$

Point C on the isotherm is again projected horizontally to meet $\overline{OA}$ at F. Also, at C a line of the equal slope as $\overline{OA}$ is projected to intercept the volume axis at G, and meet $\overline{OA}$ and the pressure axis at H and I respectively. The pressure deviation from the corresponding linear isotherm pressure is $\overline{CF} = P_a$.

$$P_a = \overline{CF} = \overline{GH} = \overline{OI} \tag{25}$$

Also,

$$\delta = \overline{CD} = \overline{GO} = \overline{HI} \tag{26}$$

Along $\overline{OA}$,

$$slope = \frac{\overline{HI}}{\overline{OI}} = \frac{\overline{AB}}{\overline{OB}} \tag{27}$$

$$\frac{\delta}{P_a} = \frac{V_{max}}{P_s} \tag{28}$$

$$\frac{\delta}{V_{max}} = \frac{P_a}{P_s} \tag{29}$$

Substituting Equation 29 into Equation 24 gives:

$$\frac{V}{V_{max}} = \frac{P}{P_s} + \frac{P_a}{P_s} \tag{30}$$

i.e.

$$V = V_{max} \left(\frac{P + P_a}{P_s} \right) \tag{31}$$

2.4 Establishment of Boundary Conditions for P_a

Boundary conditions for P_a, the pressure deviation from the corresponding linear isotherm, is highlighted thus:

1. $P_a = 0$ at $P = 0$ and $P = P_s$
2. $P_a > 0$ within the pressure range $0 < P < P_s$
3. P_a is maximum ($\frac{dP_a}{dP} = 0$) i.e. $\frac{d}{dP}\left\{(P_s - P)\left(\frac{P}{P_s}\right)^n\right\} = 0$ at the inflexion point β of the isotherm within the pressure range

6

$0 < P < P_s$. At the inflexion point β , $\Delta\left(\frac{V}{V_{max}}\right) = \Delta\left(\frac{P}{P_s}\right)$.

4. For saturated adsorption, i.e. when $P > P_s$, at J (see Fig. 3), a line of the equal slope as $\overline{OA}$ is projected to intercept the volume axis at K and meet $\overline{OA}$ extension and the pressure axis at L and M respectively.

$$P_a = \overline{OM} = \overline{KL} = -\overline{AJ} \qquad (32)$$

$$P_a = -(P - P_s) \qquad (33)$$

$$P_a = P_s - P \qquad (34)$$

and

$$V = V_{max} \qquad (35)$$

2.5 Plot of Relative Adsorbed Volume versus Relative Pressure for the Developed Adsorption Isotherm

For pressure range below adsorption saturation pressure $(P < P_s)$, the developed adsorption isotherm $\frac{V}{V_{max}} = \left\{\frac{P}{P_s} + \left(1 - \frac{P}{P_s}\right)\left(\frac{P}{P_s}\right)^n\right\}$ could be expressed as:

$$Y = \{X + (1 - X)(X)^n\} \qquad (36)$$

A plot of Y versus X is shown in Fig. 4. As stated earlier, the major representatives of Type I adsorption isotherm pressure-volume data (below the adsorption saturation pressure) are captured and depicted by the adsorbate-adsorbent resistance parameter n ranging from 0.30 to 1.15.

2.6 Parameterization of Experimental Adsorption Data Using the Developed Isotherm

The steps involved in the developed isotherm parameters evaluation from experimental data are as highlighted below:

1. Produce the experimental adsorption isotherm by plotting the adsorbed volume V versus pressure P.
2. Compare and match the experimental isotherm with the relative adsorbed volume–relative pressure curve (see Fig. 4) and select a few adsorbate-adsorbent resistance parameter n of closer range.

3. For each n selected, feature the corresponding parameters $b = \frac{V_{last}}{V_{max}}$ and $c = \frac{P_{last}}{P_s}$ (see Tables 1, 2 and 3) where P_{last}, V_{last} are the last P, V values of the experimental adsorption data. Thus evaluate the corresponding $V_{max} = \frac{V_{last}}{b}$ and $P_s = \frac{P_{last}}{c}$, and the pressure P_β, and adsorbed volume V_β at the inflexion point β where $\Delta\left(\frac{V}{V_{max}}\right) = \Delta\left(\frac{P}{P_s}\right)$ on the developed isotherm (see Table 4). Note that $\frac{V_{last}}{V_{max}} = \left\{\frac{P_{last}}{P_s} + \left(1 - \frac{P_{last}}{P_s}\right)\left(\frac{P_{last}}{P_s}\right)^n\right\}$.

The details of the evaluation of pressure P_β and adsorbed volume V_β at point β where $\Delta\left(\frac{V}{V_{max}}\right) = \Delta\left(\frac{P}{P_s}\right)$ on the developed isotherm are shown in Appendix B.

4. Choose the P_β , V_β values that correlate with the experimental adsorption isotherm, and thus consider the corresponding n, P_s and V_{max} as the parameters of the developed adsorption isotherm for the experimental adsorption data.

5. Model the experimental adsorption data as:

$$V = \begin{cases} V_{max}\left\{\frac{P}{P_s} + \left(1 - \frac{P}{P_s}\right)\left(\frac{P}{P_s}\right)^n\right\}, for\ P < P_s \\ V_{max},\ for\ P \geq P_s \end{cases} \qquad (37)$$

Where V is the adsorbed volume at equilibrium pressure P , P_s is the adsorption saturation pressure at which the maximum adsorbed volume V_{max} is attained, n is adsorbate-adsorbent resistance parameter (n ranges from 0.30 to 1.15).

2.7 Parameterization of Experimental Adsorption Data Using Langmuir Isotherm

The steps involved in Langmuir isotherm parameters evaluation from experimental data are as highlighted below:

1. Obtain the parameters V_L and P_L (Langmuir volume and Langmuir pressure respectively) by arranging the isotherm $V = V_L\left(\frac{P}{P+P_L}\right)$ thus:

$$\frac{P}{V} = \left(\frac{1}{V_L}\right) P + \left(\frac{1}{V_L}\right) P_L \qquad (38)$$

2. Plot $\frac{P}{V}$ versus P to yield the equation of a straight line: $Y = mX + C$, where slope $m = \frac{1}{V_L}$ and Y-axis intercept $C = \left(\frac{1}{V_L}\right) P_L$ are obtained from the best fit line.

3. Model the laboratory adsorption data using the two parameters V_L and P_L as:

$$V = V_L \frac{P}{P+P_L} \qquad (39)$$

2.8 Generalization of the Developed Isotherm

The step involved are as follows:

1. Plot V versus P for the experimental data, the proposed isotherm and Langmuir isotherm.

2. Correlate the developed isotherm with Langmuir isotherm and validate with the experimental data using statistical deviation (error) parameters.
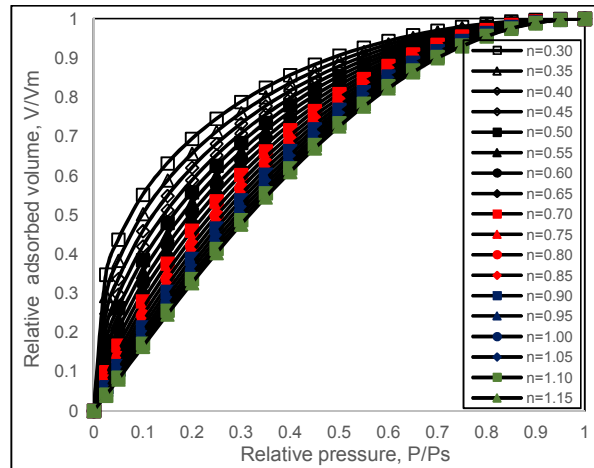

Fig. 4. Plot of relative adsorbed volume versus relative pressure for the developed adsorption isotherm

Table 1. Adsorption saturation data for establishing the boundary conditions of the developed isotherm ($n = 0.30 \ to \ 0.55$)

$b = \dfrac{V_{last}}{V_{max}}$	$n = 0.30$ $c = \dfrac{P_{last}}{P_s}$	$n = 0.35$ $c = \dfrac{P_{last}}{P_s}$	$n = 0.40$ $c = \dfrac{P_{last}}{P_s}$	$n = 0.45$ $c = \dfrac{P_{last}}{P_s}$	$n = 0.50$ $c = \dfrac{P_{last}}{P_s}$	$n = 0.55$ $c = \dfrac{P_{last}}{P_s}$
0.920	0.5339	0.5621	0.5853	0.6049	0.6218	0.6365
0.925	0.5470	0.5746	0.5974	0.6166	0.6331	0.6474
0.930	0.5607	0.5877	0.6100	0.6287	0.6448	0.6588
0.935	0.5751	0.6014	0.6231	0.6413	0.6570	0.6706
0.940	0.5901	0.6157	0.6368	0.6545	0.6697	0.6830
0.945	0.6060	0.6308	0.6512	0.6684	0.6831	0.6959
0.950	0.6227	0.6467	0.6664	0.6830	0.6972	0.7095
0.955	0.6405	0.6636	0.6825	0.6984	0.7120	0.7238
0.960	0.6594	0.6815	0.6996	0.7148	0.7278	0.7390
0.965	0.6799	0.7009	0.7180	0.7324	0.7447	0.7553
0.970	0.7021	0.7218	0.7380	0.7514	0.7629	0.7730
0.975	0.7265	0.7449	0.7598	0.7723	0.7830	0.7922
0.980	0.7539	0.7706	0.7842	0.7956	0.8052	0.8136
0.985	0.7855	0.8002	0.8122	0.8222	0.8307	0.8381
0.990	0.8235	0.8358	0.8458	0.8541	0.8612	0.8673
0.995	0.8739	0.8829	0.8902	0.8962	0.9013	0.9057
1.000	1.0000	1.0000	1.0000	1.0000	1.0000	1.0000

Table 2. Adsorption saturation data for establishing the boundary conditions of the developed isotherm ($n = 0.60\ to\ 0.85$)

$b = \dfrac{V_{last}}{V_{max}}$	$n = 0.60$ $c = \dfrac{P_{last}}{P_s}$	$n = 0.65$ $c = \dfrac{P_{last}}{P_s}$	$n = 0.70$ $c = \dfrac{P_{last}}{P_s}$	$n = 0.75$ $c = \dfrac{P_{last}}{P_s}$	$n = 0.80$ $c = \dfrac{P_{last}}{P_s}$	$n = 0.85$ $c = \dfrac{P_{last}}{P_s}$
0.920	0.6495	0.6610	0.6714	0.6808	0.6893	0.6972
0.925	0.6601	0.6714	0.6815	0.6907	0.6990	0.7066
0.930	0.6711	0.6821	0.6920	0.7009	0.7090	0.7165
0.935	0.6826	0.6933	0.7029	0.7116	0.7194	0.7266
0.940	0.6946	0.7050	0.7142	0.7226	0.7303	0.7372
0.945	0.7071	0.7171	0.7261	0.7342	0.7416	0.7483
0.950	0.7203	0.7299	0.7385	0.7463	0.7534	0.7599
0.955	0.7342	0.7434	0.7517	0.7591	0.7659	0.7721
0.960	0.7489	0.7577	0.7656	0.7727	0.7791	0.7850
0.965	0.7647	0.7730	0.7804	0.7871	0.7932	0.7988
0.970	0.7817	0.7895	0.7964	0.8027	0.8084	0.8136
0.975	0.8003	0.8075	0.8139	0.8197	0.8249	0.8297
0.980	0.8210	0.8274	0.8333	0.8385	0.8432	0.8476
0.985	0.8445	0.8502	0.8553	0.8599	0.8641	0.8679
0.990	0.8727	0.8774	0.8816	0.8854	0.8889	0.8920
0.995	0.9096	0.9130	0.9161	0.9188	0.9213	0.9236
1.000	1.0000	1.0000	1.0000	1.0000	1.0000	1.0000

Table 3. Adsorption saturation data for establishing the boundary conditions of the developed isotherm ($n = 0.90\ to\ 1.15$)

$b = \dfrac{V_{last}}{V_{max}}$	$n = 0.90$ $c = \dfrac{P_{last}}{P_s}$	$n = 0.95$ $c = \dfrac{P_{last}}{P_s}$	$n = 1.00$ $c = \dfrac{P_{last}}{P_s}$	$n = 1.05$ $c = \dfrac{P_{last}}{P_s}$	$n = 1.10$ $c = \dfrac{P_{last}}{P_s}$	$n = 1.15$ $c = \dfrac{P_{last}}{P_s}$
0.920	0.7044	0.7110	0.7172	0.7230	0.7283	0.7334
0.925	0.7136	0.7202	0.7262	0.7318	0.7370	0.7420
0.930	0.7233	0.7296	0.7355	0.7409	0.7460	0.7508
0.935	0.7333	0.7394	0.7451	0.7504	0.7553	0.7600
0.940	0.7437	0.7496	0.7551	0.7602	0.7650	0.7695
0.945	0.7545	0.7602	0.7665	0.7705	0.7751	0.7794
0.950	0.7658	0.7713	0.7764	0.7812	0.7856	0.7898
0.955	0.7778	0.7830	0.7879	0.7925	0.7967	0.8006
0.960	0.7904	0.7954	0.8000	0.8044	0.8084	0.8121
0.965	0.8039	0.8086	0.8130	0.8170	0.8208	0.8244
0.970	0.8184	0.8228	0.8268	0.8306	0.8342	0.8375
0.975	0.8341	0.8382	0.8419	0.8454	0.8487	0.8517
0.980	0.8516	0.8552	0.8586	0.8618	0.8647	0.8675
0.985	0.8714	0.8746	0.8776	0.8803	0.8829	0.8853
0.990	0.8949	0.8976	0.9000	0.9023	0.9045	0.9065
0.995	0.9257	0.9276	0.9293	0.9310	0.9325	0.9339
1.000	1.0000	1.0000	1.0000	1.0000	1.0000	1.0000

2.9 Statement of Developed Isotherm for Gas Mixture

Concerning the pure-component adsorption isotherm developed in this study, the volume of the adsorbing specie i in a mixture of gases at an equilibrium pressure P is expressed:

$$V_i = \left(\frac{y_i (V_{max})_i}{\sum_{j=1}^{N} y_j (V_{max})_j}\right) * (V_{100\%})_i \tag{40}$$

Where, y_i is the gas-phase mole fraction (or the feed ratio) of the adsorbing specie i; $(V_{max})_i$ is the maximum adsorbed volume of the adsorbing specie i of 100% concentration; y_j is the

9

Table 4. P-V parameters at point β where $\Delta\left(\frac{V}{V_{max}}\right) = \Delta\left(\frac{P}{P_s}\right)$

	$n = 0.30$	$n = 0.35$	$n = 0.40$	$n = 0.45$	$n = 0.50$	$n = 0.55$
$P_\beta = \frac{n}{n+1}P_s$	$\frac{3}{13}P_s$	$\frac{7}{27}P_s$	$\frac{2}{7}P_s$	$\frac{9}{29}P_s$	$\frac{1}{3}P_s$	$\frac{11}{31}P_s$
V_β	$0.7262V_{max}$	$0.7211V_{max}$	$0.7185V_{max}$	$0.7177V_{max}$	$0.7182V_{max}$	$0.7197V_{max}$
	$n = 0.60$	$n = 0.65$	$n = 0.70$	$n = 0.75$	$n = 0.80$	$n = 0.85$
$P_\beta = \frac{n}{n+1}P_s$	$\frac{3}{8}P_s$	$\frac{13}{33}P_s$	$\frac{7}{17}P_s$	$\frac{3}{7}P_s$	$\frac{4}{9}P_s$	$\frac{17}{37}P_s$
V_β	$0.7220V_{max}$	$0.7247V_{max}$	$0.7278V_{max}$	$0.7312V_{max}$	$0.7348V_{max}$	$0.7385V_{max}$
	$n = 0.90$	$n = 0.95$	$n = 1.00$	$n = 1.05$	$n = 1.10$	$n = 1.15$
$P_\beta = \frac{n}{n+1}P_s$	$\frac{9}{19}P_s$	$\frac{19}{39}P_s$	$\frac{1}{2}P_s$	$\frac{21}{41}P_s$	$\frac{11}{21}P_s$	$\frac{23}{43}P_s$
V_β	$0.7423V_{max}$	$0.7462V_{max}$	$0.7500V_{max}$	$0.7538V_{max}$	$0.7576V_{max}$	$0.7614V_{max}$

gas-phase mole fraction (or the feed ratio) of the respective specie j ; $(V_{max})_j$ is maximum adsorbed volume of the respective specie j of 100% concentration; $j = 1, ... N$; N is the number of gas specie; $(V_{100\%})_i$ is the volume of the adsorbing specie i of 100% concentration at the corresponding pressure.

2.10 Correlation of the Developed Isotherm for Gas Mixture with the Extended Langmuir Isotherm

The mixing rule for the developed adsorption isotherm (for gas mixture) is correlated with the extended Langmuir isotherm expressed as:

$$V_i = (V_L)_i \frac{y_i b_i P}{\left(1 + \sum_{j=1}^{N} y_j b_j P\right)} \qquad (41)$$

Where, y_i is the gas-phase mole fraction of the adsorbing specie i ; b_i is equal to $1/P_{L_i}$, the temperature-dependent pure-component Langmuir model parameter;; P is equilibrium pressure; and $j = 1, ... N$; N is the number of gas component.

2.11 Statistical Deviation (Error) Parameters Used

The statistical deviation (error) parameters used in assessing the quality of fit in the adsorption model representation are the weighted root mean square (WRMS) deviation, the weighted average absolute deviation (WAAD), the per cent average absolute deviation (%AAD) and the root mean square error (RMSE). These parameters are expressed as follows:

$$WRMS = \sqrt{\frac{1}{N} \cdot \sum_{i=1}^{N} \left(\frac{V_{cal} - V_{exp}}{\sigma_{exp}}\right)_i^2} \qquad (42)$$

$$WAAD = \frac{1}{N} \cdot \sum_{i=1}^{N} abs \left(\frac{V_{cal} - V_{exp}}{\sigma_{exp}}\right)_i \qquad (43)$$

$$\%AAD = \frac{1}{N} \cdot \sum_{i=1}^{N} abs \left(\frac{V_{cal} - V_{exp}}{V_{exp}}\right)_i \times 100\% \quad (44)$$

and

$$RMSE = \sqrt{\frac{1}{N} \cdot \sum_{i=1}^{N} \left(V_{cal} - V_{exp}\right)_i^2} \qquad (45)$$

Here, i is the data point, N is the number of data points, V_{exp} is the experimental adsorption volume, V_{cal} is the calculated adsorption volume and σ_{exp} is the expected experimental uncertainty.

3. RESULTS AND DISCUSSION

3.1 Experimental Pure Gas Adsorption Data Employed

The developed isotherm can be used to model all cases of monolayer adsorptions of gases (or fluids) on adsorbents. However, in this research work, experimental pure gas adsorption data employed are highlighted in Tables 5, 6 and 7 where the absolute uncertainty in adsorption is denoted as σ_{Exp}.

3.2 Methane Adsorption on Turkey's Shale Sample at 25°C (Source: Merey, 2013)

3.2.1 Parameterisation of methane adsorption on Turkey's shale sample at 25°C using the developed isotherm

Plotting the experimental isotherm from Table 5 and matching it with the relative adsorbed

volume – relative pressure curve (see Fig. 4.) shows n to be in the range of 0.35 to 0.45. For each n, the corresponding parameters $b = \frac{V_{last}}{V_{max}}$ and $c = \frac{P_{last}}{P_s}$ were featured. Using Excel spreadsheet programming; the corresponding $V_{max} = \frac{V_{last}}{b}$ and $P_s = \frac{P_{last}}{c}$, and the pressure and adsorbed volume at the inflexion point β where $\Delta\left(\frac{V}{V_{max}}\right) = \Delta\left(\frac{P}{P_s}\right)$ on the isotherms were evaluated. The adsorption resistance parameter $n = 0.40$ yields the P_β, V_β values that correlate with the experimental adsorption isotherm as shown in Table 8.

The P_β, V_β values of 572 psia and 0.0323 mmol/g correlate with the experimental isotherm

(see Fig. 5) and the corresponding P_s, V_{max} values 2005 psia and 0.0450 mmol/g is considered as the developed isotherm parameters for the experimental adsorption data.

Hence, methane adsorption on Turkey's shale sample at 25°C is modelled as:

$$V\ (mmol/g) = \left\{ \begin{matrix} 0.0450 \left\{ \frac{P}{2005} + \left(1 - \frac{P}{2005}\right) \frac{P}{2005}^{\,0.40} \right\}, P < 2005\ psia \\ 0.0450\ , P \geq 2005\ psia \end{matrix} \right\} \quad (46)$$

Where, maximum adsorbed volume $V_{max} = 0.0450\ mmol/g$, adsorption saturation pressure $P_s = 2005\ psia$, and $n = 0.40$ is a parameter that defines the Turkey's shale sample resistance to methane at 25°C.

Table 5. Pure methane adsorption on Turkey's shale sample at 25ºC (i.e. 77ºF)

Pressure, P (psia)	Gibbs adsorption, V (mmol g^{-1})	σ_{Exp} (mmol g^{-1})
190	0.0197	0.0024
403	0.0265	0.0037
602	0.0325	0.0050
805	0.0361	0.0063
1002	0.0394	0.0077
1201	0.0412	0.0092
1403	0.0437	0.0107
1598	0.0446	0.0122
1798	0.0447	0.0137
2005	0.0450	0.0153

Source: [27]

Table 6. Pure methane adsorption on dry tiffany mixed coal sample at 130°F

Pressure, P (psia)	Absolute adsorption, V (scf/ton)	σ_{Exp} (scf/ton)
255.9	117.0	3.510
824.9	243.9	7.317
1210.2	283.6	8.508
1796.9	316.6	9.498

Source: [34]; Note: σ_{Exp} were evaluated based on average expected experimental uncertainty of 3%

Table 7. Pure nitrogen adsorption on dry tiffany mixed coal sample at 130°F

Pressure, P (psia)	Absolute adsorption, V (scf/ton)	σ_{Exp} (scf/ton)
106.6	18.1	1.086
202.9	29.9	1.794
406.0	52.9	3.174
602.7	69.7	4.182
795.6	88.1	5.286
1000.2	102.3	6.138
1202.5	113.9	6.834
1410.9	126.6	7.596
1604.9	138.0	8.280
1806.2	147.2	8.832

Source: [34]; Note: σ_{Exp} were evaluated based on average expected experimental uncertainty of 6%

Table 8. Adsorption saturation data for establishing the boundary conditions of the developed isotherm for methane adsorption on Turkey's shale sample at 25°C (Here, $V_{last} = 0.0450 \, mmol/g$ and $P_{last} = 2005 \, psia$)

$b = \dfrac{V_{last}}{V_{max}}$	$n = 0.40$					
	$c = \dfrac{P_{last}}{P_s}$	$V_{max} = \dfrac{V_{last}}{b}$ (mmol/g)	$P_s = \dfrac{P_{last}}{c}$ (psia)	$V_\beta = 0.7185 V_{max}$ (mmol/g)	$P_\beta = \dfrac{2}{7} P_s$ (psia)
0.955	0.6825	0.0471	2938	0.0338	839
0.960	0.6996	0.0469	2866	0.0337	819
0.965	0.7180	0.0466	2793	0.0335	798
0.970	0.7380	0.0464	2717	0.0333	776
0.975	0.7598	0.0461	2639	0.0331	754
0.980	0.7842	0.0459	2557	0.0330	731
0.985	0.8122	0.0457	2469	0.0328	705
0.990	0.8458	0.0454	23721	0.0326	677
0.995	0.8902	0.0452	2252	0.0325	643
1.000	1.000	0.0450	2005	0.0323	572
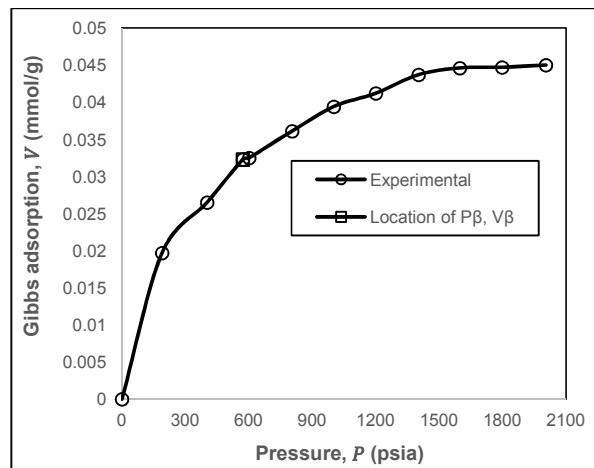
Fig. 5. Location of P_β, V_β correlation on the experimental isotherm for methane adsorption on Turkey's shale sample B at 25°C

Table 9. Prediction of methane adsorption on Turkey's shale sample at 25°C using the developed isotherm

Pressure, P (psia)	Gibbs adsorption, V (mmol/g)		Deviation (Error) analysis			
	Experimental	Developed isotherm	σ_{Exp} (mmol/g)	$V_{Cal} - V_{Exp}$ (mmol/g)	$\dfrac{V_{Cal} - V_{Exp}}{\sigma_{Exp}}$	$\dfrac{V_{Cal} - V_{Exp}}{V_{Exp}}$
190	0.0197	0.0201	0.0024	0.0004	0.1667	0.0203
403	0.0265	0.0280	0.0037	0.0015	0.4054	0.0566
602	0.0325	0.0330	0.0050	0.0005	0.1000	0.0154
805	0.0361	0.0368	0.0063	0.0007	0.1111	0.0194
1002	0.0394	0.0395	0.0077	0.0001	0.0130	0.0025
1201	0.0412	0.0417	0.0092	0.0005	0.0543	0.0121
1403	0.0437	0.0432	0.0107	-0.0005	-0.0467	-0.0114
1598	0.0446	0.0442	0.0122	-0.0004	-0.0330	-0.0090
1798	0.0447	0.0448	0.0137	0.0001	0.0073	0.0022
2005	0.0450	0.0450	0.0153	0	0	0

Here, weighted root mean square, WRMS = 0.1486, weighted average absolute deviation, WAAD = 0.0937, percent average absolute deviation, %AAD = 1.4890, root mean square error, RMSE = 0.0006 mmol/g and R^2 value = 0.9973

3.2.2 Prediction of methane adsorption on Turkey's shale sample at 25°C using the developed isotherm

Prediction of methane adsorption on Turkey's shale sample at 25°C using the developed isotherm, and the corresponding deviation/error analysis parameters are presented in Table 9.

3.2.3 Parameterization of methane adsorption on Turkey's shale sample at 25°C using langmuir isotherm

The variations of P/V versus P for methane adsorption on Turkey's shale sample at 25°C is shown in Table 10.

The best fit line of the plot of P/V versus P (shown in Fig. 6) yields the equation: $Y = 18.261x + 7081.4$ with R^2 of 0.9952, where slope

$m = 18.261 = 1/V_L$ and Y-axis intercept $C = 7081.4 = \frac{1}{V_L}P_L$.

Here, Langmuir volume V_L and Langmuir pressure P_L are respectively obtained as 0.0548 mmol/g and 387.79 psia. Hence, methane adsorption on Turkey's shale sample at 25°C is modelled as:

$$V = 0.0548 * \frac{P}{P+387.79} \qquad mmol/g \qquad (47)$$

where Langmuir constant $b = \frac{1}{P_L} = 0.002579\ psia^{-1}$.

3.2.4 Prediction of methane adsorption on Turkey's shale sample at 25°C using langmuir isotherm

Prediction of methane adsorption on Turkey's shale sample at 25°C using Langmuir isotherm, and the corresponding deviation/error analysis parameters are presented in Table 11.

Table 10. Parameters for plotting Langmuir isotherm for methane adsorption on Turkey's shale sample at 25°C

Experimental		$\frac{Pressure}{Volume}$, P/V (psia/mmol/g)
Pressure, P (psia)	Gibbs adsorption, V (mmol/g)	
190	0.0197	9645
403	0.0265	15207
602	0.0325	18523
805	0.0361	22230
1002	0.0394	25431
1201	0.0412	29150
1403	0.0437	32105
1598	0.0446	34739
1798	0.0447	40224
2005	0.0450	44556
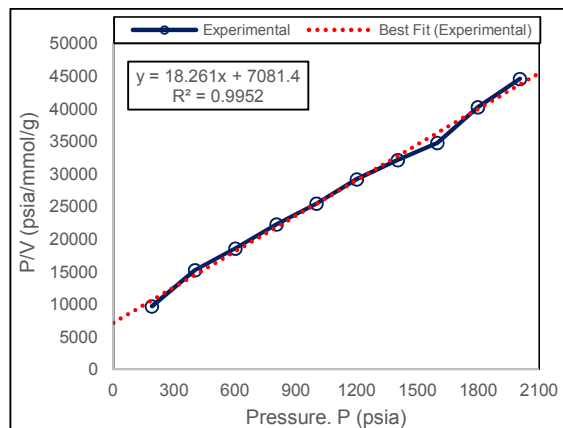
Fig. 6. Plot of $\frac{P}{V}$ versus P for methane adsorption on Turkey's shale sample at 25°C
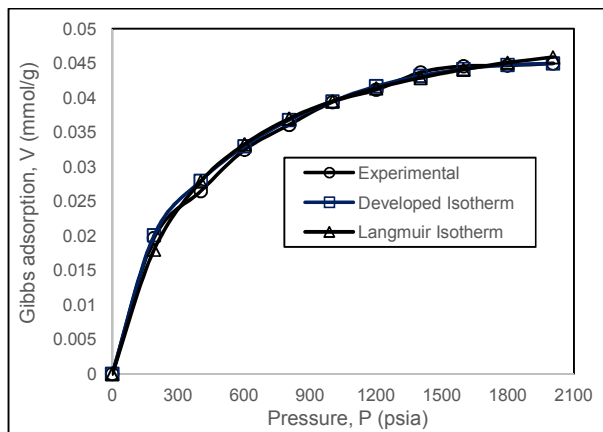
Table 11. Prediction of methane adsorption on Turkey's shale sample at 25°C using Langmuir isotherm

Pressure, P (psia)	Gibbs adsorption, V (mmol/g)		Deviation (Error) analysis			
	Experimental	Langmuir Isotherm	σ_{Exp} (mmol/g)	$V_{Cal} - V_{Exp}$ (mmol/g)	$\dfrac{V_{Cal} - V_{Exp}}{\sigma_{Exp}}$	$\dfrac{V_{Cal} - V_{Exp}}{V_{Exp}}$
190	0.0197	0.0180	0.0024	-0.0017	-0.7083	-0.0863
403	0.0265	0.0279	0.0037	0.0014	0.3784	0.0528
602	0.0325	0.0333	0.0050	0.0008	0.1600	0.0246
805	0.0361	0.0370	0.0063	0.0009	0.1429	0.0249
1002	0.0394	0.0395	0.0077	0.0001	0.0130	0.0025
1201	0.0412	0.0414	0.0092	0.0002	0.0217	0.0049
1403	0.0437	0.0429	0.0107	-0.0008	-0.0748	-0.0183
1598	0.0446	0.0441	0.0122	-0.0005	-0.0410	-0.0112
1798	0.0447	0.0451	0.0137	0.0004	0.0292	0.0089
2005	0.0450	0.0459	0.0153	0.0009	0.0588	0.0200

Here, weighted root mean square, WRMS = 0.2652, weighted average absolute deviation, WAAD = 0.1628, percent average absolute deviation, %AAD = 2.5440, root mean square error, RMSE = 0.0009 mmol/g and R^2 value = 0.9891

Table 12. Generalization of the developed isotherm for methane adsorption on Turkey's shale sample at 25°C

Pressure, P (psia)	Gibbs adsorption, V (mmol/g)		
	Experimental	Developed Isotherm	Langmuir Isotherm
190	0.0197	0.0201	0.0180
403	0.0265	0.0280	0.0279
602	0.0325	0.0330	0.0333
805	0.0361	0.0368	0.0370
1002	0.0394	0.0395	0.0395
1201	0.0412	0.0417	0.0414
1403	0.0437	0.0432	0.0429
1598	0.0446	0.0442	0.0441
1798	0.0447	0.0448	0.0451
2005	0.0450	0.0450	0.0459

Fig. 7. Generalization of the developed isotherm for methane adsorption on Turkey's shale sample at 25

Table 13. Langmuir and the developed predictions of methane adsorption on Turkey's shale sample at 25°C for high-pressure range

Pressure, P (psia)	Gibbs adsorption, V (mmol/g)	
	Developed Isotherm	Langmuir Isotherm
190	0.0201	0.0180
602	0.0330	0.0333
1002	0.0395	0.0395
1403	0.0432	0.0429
1798	0.0448	0.0451
2005	0.0450	0.0459
2400	0.0450	0.0472
2800	0.0450	0.0481
3200	0.0450	0.0489
3600	0.0450	0.0495
4000	0.0450	0.0500
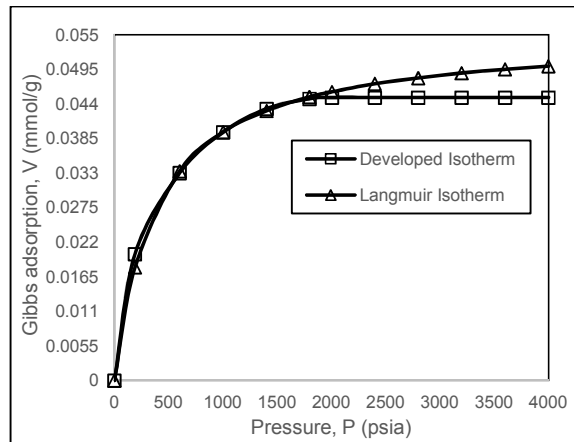
Fig. 8. Predictions of methane adsorption on Turkey's shale sample at 25°C for high-pressure range by the developed and Langmuir isotherms

3.2.5 The generalisation of the developed isotherm for methane adsorption on Turkey's shale sample at 25°C

To validate and generalize the developed isotherm, predictions of methane adsorption on Turkey's shale sample at 25°C by Langmuir and the developed isotherms are correlated with the experimental data as shown in Table 12 and Fig. 7.

3.2.6 Comparison of high-pressure adsorption predictions for methane adsorption on Turkey's shale sample at 25°C

Langmuir and the developed isotherms predictions of methane adsorption on Turkey's shale sample at 25°C for the high-pressure range are compared in Table 13 and Fig. 8.

The developed isotherm predicts a maximum adsorption volume of 0.0450 mmol/g at adsorption saturated pressure of 2005 psia. However, by Langmuir isotherm prediction, a maximum adsorption volume of 0.0548 mmol/g is attained at infinite adsorption saturated pressure. Fig. 7 shows that adsorption prediction by Langmuir isotherm is not reliable at higher pressures because of its inefficiency in defining the onset of adsorption saturation pressure; this contributes to an overestimation of maximum adsorbed volume.

3.2.7 Methane adsorption on Tiffany mixed coal sample at 130°F (Source: Gasem et al., 2002) parameterization of methane adsorption on Tiffany mixed coal sample at 130°F

Plotting the experimental isotherm from Table 6 and matching it with the relative adsorbed

15

volume – relative pressure curve (see Fig. 4) shows n to be in the range of 0.45 to 0.55. For each n, the corresponding parameters $b = \frac{V_{last}}{V_{max}}$ and $c = \frac{P_{last}}{P_s}$ were featured. Using *Excel* spreadsheet programming; the corresponding $V_{max} = \frac{V_{last}}{b}$ and $P_s = \frac{P_{last}}{c}$ and the pressure and adsorbed volume at the inflexion point β where $\Delta\left(\frac{V}{V_{max}}\right) = \Delta\left(\frac{P}{P_s}\right)$ on the isotherms were evaluated. The adsorption resistance parameter $n = 0.40$ yields the P_β, V_β values that correlate with the experimental adsorption isotherm as shown in Table 14.

The P_β, V_β values of 765.0 psia and 233.2 scf/ton correlate with the experimental isotherm (see

Fig. 9), and the corresponding P_s, V_{max} values of 2294.9 psia and 324.7 scf/ton are considered as the developed isotherm parameters for the experimental adsorption data.
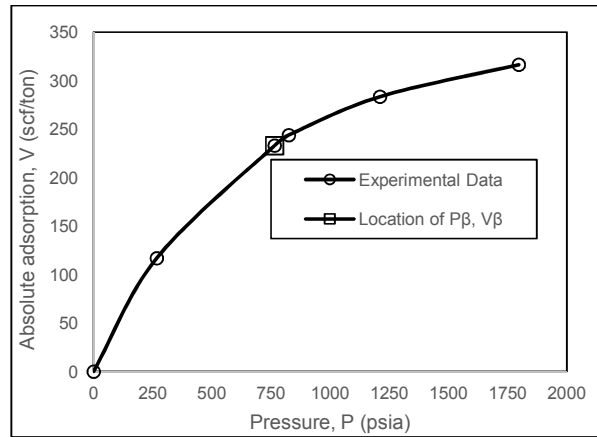
Hence, pure methane adsorption on dry Tiffany mixed coal sample at 130°F is modelled as:

$$V(scf/ton) = \left\{\begin{array}{l} 324.7\left\{\frac{P}{2294.9} + \left(1 - \frac{P}{2294.9}\right)\left(\frac{P}{2294.9}\right)^{0.50}\right\}, for\ P < 2294.9\ psia \\ 324.7,\ for\ P \geq 2294.9\ psia \end{array}\right\} \quad (48)$$

Where, maximum adsorbed volume V_{max} = 324.7 scf/ton, adsorption saturation pressure P_s = 2294.9 psia, and n = 0.50 is a parameter that defines dry Tiffany mixed coal sample resistance to pure methane adsorption at 130°F.

Table 14. Adsorption saturation data for establishing the boundary conditions of the developed isotherm for pure methane adsorption on dry tiffany mixed coal sample at 130°F (Here, V_{last} = 316.6 scf/ton and P_{last} = 1,796.9 psia)

$b = \frac{V_{last}}{V_{max}}$	$c = \frac{P_{last}}{P_s}$	$V_{max} = \frac{V_{last}}{b}$ (scf/ton)	$P_s = \frac{P_{last}}{c}$ (psia)	$V_\beta = 0.7182V_{max}$ (scf/ton)	$P_\beta = \frac{1}{3}P_s$ (psia)
0.955	0.7120	331.5	2523.7	238.1	841.2
0.960	0.7278	329.8	2468.9	236.9	823.0
0.965	0.7447	328.1	2412.9	235.6	804.3
0.970	0.7629	326.4	2355.3	234.4	785.1
0.975	0.7830	324.7	2294.9	233.2	765.0
0.980	0.8052	323.1	2231.6	232.0	743.9
0.985	0.8307	321.4	2163.1	230.8	721.0
0.990	0.8612	319.8	2086.6	229.7	695.5
0.005	0.9013	318.2	1993.7	228.5	664.6
1.000	1.0000	316.6	1796.9	227.4	599.0

Fig. 9. Location of P_β, V_β correlation on the experimental isotherm for pure methane adsorption on dry tiffany mixed coal sample at 130°F
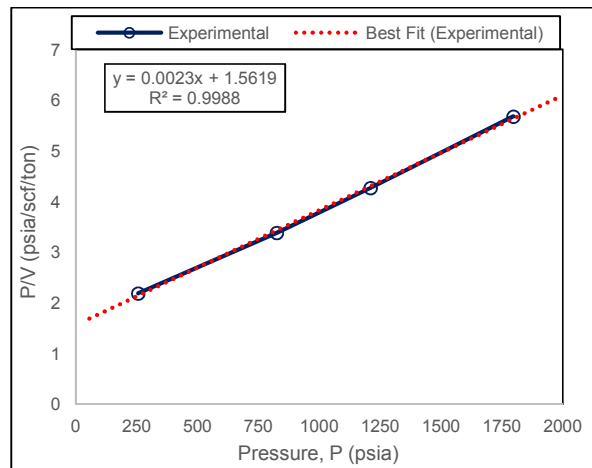
Table 15. Prediction of pure methane adsorption on dry tiffany mixed coal sample at 130°F using the developed isotherm

Pressure, P (psia)	Absolute adsorption, V (scf/ton)		Deviation (Error) analysis			
	Experimental	**Developed isotherm**	σ_{Exp} (scf/ton)	$V_{Cal} - V_{Exp}$ (scf/ton)	$\dfrac{V_{Cal} - V_{Exp}}{\sigma_{Exp}}$	$\dfrac{V_{Cal} - V_{Exp}}{V_{Exp}}$
255.9	117.0	132.5	3.510	15.5	4.416	0.132
824.9	243.9	241.4	7.317	-2.5	-0.342	-0.010
1210.2	283.6	282.7	8.508	-0.9	-0.106	-0.003
1796.9	316.6	316.6	9.498	0	0	0

Here, weighted root mean square, WRMS = 2.2152, weighted average absolute deviation, WAAD = 1.2160, percent average absolute deviation, %AAD = 3.6250, root mean square error, RMSE = 7.8630 scf/ton and R^2 value = 0.9977

Table 16. Parameters for plotting Langmuir isotherm for pure methane adsorption on dry tiffany mixed coal sample at 130°F

Experimental		$\dfrac{Pressure}{Volume}, P/V$ (psia/scf/ton)
Pressure, P (psiaa)	**Absolute adsorption, V (scf/ton)**	
255.9	117.0	2.1872
824.9	243.9	3.3821
1210.2	283.6	4.2673
1796.9	316.6	5.6756

Fig. 10. Plot of P/V versus P for pure methane adsorption on dry tiffany mixed coal sample at 130°F

3.2.8 Prediction of methane adsorption on dry tiffany mixed coal sample at 130°F using the developed isotherm

Prediction of pure methane adsorption on dry Tiffany mixed coal sample at 130°F using the developed isotherm, and the corresponding deviation (error) analysis parameters are presented in Table 15.

3.2.9 Parameterization of pure methane adsorption on dry tiffany mixed coal sample at 130°F using langmuir isotherm

The variation of P/V with P for pure methane adsorption on dry Tiffany mixed coal sample at 130°F is shown in Table 16 and the best fit line of the plot of P/V versus P (shown in Fig. 10)

yields the equation: $y = 0.0023x + 1.5619$ with R^2 value of 0.9988, where slope $m = 0.0023 = \frac{1}{V_L}$ and Y-axis intercept $C = 1.5619 = \left(\frac{1}{V_L}\right)P_L$.

Here, Langmuir volume V_L and Langmuir pressure P_L are respectively obtained as 434.78 scf/ton and 679.09 psia. Hence, pure methane adsorption on dry Tiffany mixed coal sample at 130 °F is modelled as:

$$V(scf/ton) = 434.78\left(\frac{P}{P+679.09}\right) \qquad (49)$$

where P is pressure (psia) and Langmuir constant $b = \frac{1}{P_L} = 0.001473$ psia^{-1}.

3.2.10 Prediction of pure methane adsorption on dry Tiffany mixed coal sample at 130°F using Langmuir isotherm

Prediction of pure methane adsorption on dry Tiffany mixed coal sample at 130°F using Langmuir isotherm, and the corresponding

deviation (error) analysis parameters are presented in Table 17.

3.2.11 The generalisation of the developed Isotherm for pure methane adsorption on dry tiffany mixed coal sample at 130°F

To validate and generalise the developed isotherm, predictions of pure methane adsorption on dry Tiffany mixed coal sample at 130°F by Langmuir and the developed isotherms are correlated with the experimental data as shown in Table 18 and Fig. 11.

3.2.12 Comparison of high-pressure adsorption prediction for pure methane adsorption on dry tiffany mixed coal sample at 130°F

Langmuir and the developed isotherms predictions of pure methane adsorption on dry Tiffany mixed coal at 130°F for high-pressure range are compared in Table 19 and Fig. 12.

Table 17. Prediction of pure methane adsorption on dry tiffany mixed coal sample at 130°F using Langmuir isotherm

Pressure, P (psia)	Absolute adsorption, V (scf/ton)		Deviation (Error) analysis			
	Experimental	Langmuir isotherm	σ_{Exp} (scf/ton)	$V_{Cal} - V_{Exp}$ (scf/ton)	$\dfrac{V_{Cal} - V_{Exp}}{\sigma_{Exp}}$	$\dfrac{V_{Cal} - V_{Exp}}{V_{Exp}}$
255.9	117.0	119.0	3.510	2.000	0.570	0.017
824.9	243.9	238.5	7.317	-5.400	-0.738	-0.022
1210.2	283.6	278.5	8.508	-5.100	-0.599	-0.018
1796.9	316.6	315.5	9.498	-1.100	-0.116	-0.003

Here, weighted root mean square, WRMS = 0.5572, weighted average absolute deviation, WAAD = 0.5058, percent average absolute deviation, % AAD = 1.5000, root mean square error, RMSE = 3.8852 scf/ton and R^2 value = 0.9989
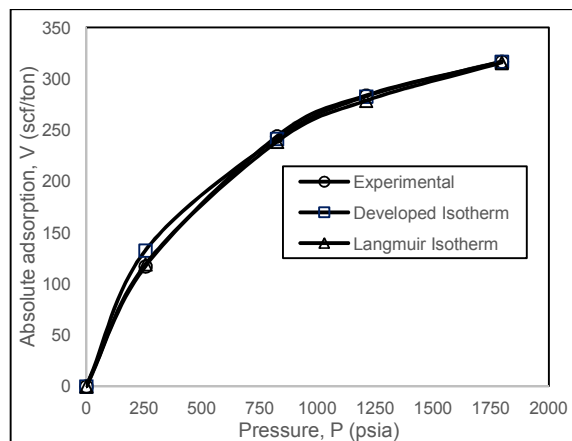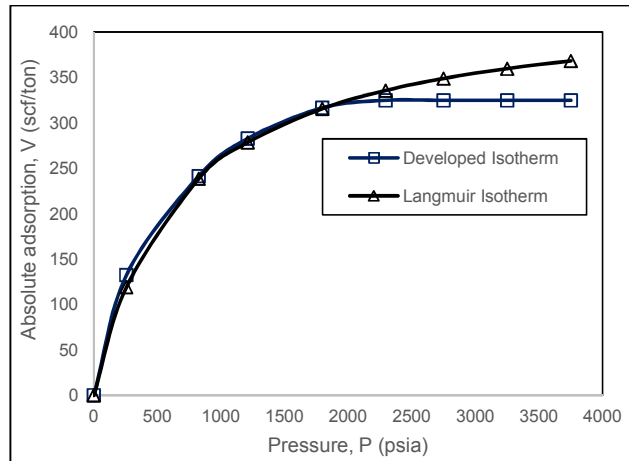

Fig. 11. Generalisation of the developed isotherm for pure methane adsorption on dry tiffany mixed coal sample at 130°F

Table 18. Generalisation of the developed isotherm for pure methane adsorption on dry tiffany mixed coal sample at 130°F

Pressure, P (psia)	Absolute adsorption, V (scf/ton)		
	Experimental	Developed isotherm	Langmuir isotherm
255.9	117.0	132.5	119.0
824.9	243.9	241.4	238.5
1210.2	283.6	282.7	278.5
1796.9	316.6	316.6	315.5

Table 19. Langmuir and the developed isotherms predictions of pure methane adsorption on dry tiffany mixed coal sample at 130°F for high-pressure range

Pressure, P (psia)	Absolute adsorption, V (scf/ton)	
	Developed isotherm	Langmuir isotherm
255.9	132.5	119.0
824.9	241.4	238.5
1210.2	282.7	278.5
1796.9	316.6	315.5
2294.9	324.7	335.5
2750	324.7	348.7
3250	324.7	359.6
3750	324.7	368.1

Fig. 12. Langmuir and the developed isotherms predictions of pure methane adsorption on dry tiffany mixed coal sample at 130°F for large pressure range

The developed isotherm predicts a maximum adsorbed volume of 324.7 scf/ton at an adsorption saturation pressure of 2294.9 psia. However, by Langmuir isotherm prediction, a maximum adsorbed volume of 434.78 scf/ton is attained at an infinite adsorption saturation pressure. Fig. 12 shows that adsorption prediction by Langmuir isotherm is not reliable at higher pressures because of its inefficiency in defining the onset of adsorption saturation pressure; this contributes to an overestimation of maximum adsorbed volume.

3.2.13 Competitive (Gas mixture) adsorptions methane and nitrogen (binary) adsorptions on tiffany mixed coal sample at 130°F

Following the steps of experimental adsorption data parameterization using the developed isotherm (highlighted above), pure nitrogen

adsorption on dry Tiffany mixed coal at 130°F (see Table 7) is modelled as:

$$V\,(scf/ton) = \begin{cases} 158.3\left\{\frac{P}{2455.7} + \left(1 - \frac{P}{2455.7}\right)\left(\frac{P}{2455.7}\right)^{1.00}\right\}, P < 2455.7\ psia \\ 158.3, P \geq 2455.7\ psia \end{cases} \quad (50)$$

where maximum adsorbed volume $V_{max} = 158.3\ scf/ton$, adsorption saturation pressure $P_s = 2455.7\ psia$ and $n = 1.00$ is a parameter that defines the dry Tiffany mixed coal resistance to pure nitrogen adsorption at 130°F.

And Langmuir isotherm modelling of the same pure nitrogen adsorption is expressed as:

$$V = 277.78 * \frac{P}{P+1689.92} \qquad scf/ton \quad (51)$$

where Langmuir constant $b = \frac{1}{P_L} = 0.0005917\ psia^{-1}$

However, adsorbed gas is often multi-component and each gas competes for the same sorption sites. For methane and nitrogen, competitive adsorptions on Tiffany mixed coal sample at 130°F, the mixing rule for the developed adsorption isotherm (see Equation 40) is correlated with extended Langmuir isotherm (see Equation 41) and validated by the laboratory measurement to generalise it.

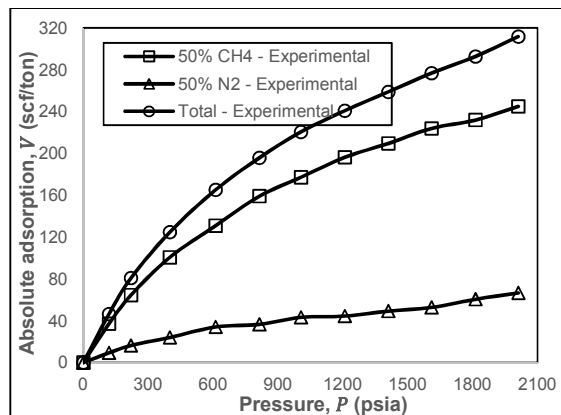### 3.2.14 Adsorption of 50% CH$_4$ - 50% N$_2$ on tiffany mixed coal sample at 130°F

The laboratory measurement of the competitive adsorption of 50% methane and 50% nitrogen on Tiffany mixed coal sample at 130°F [34] are shown in Table 20 and Fig. 13.

The single-component adsorptions of methane and nitrogen and the corresponding competitive adsorptions on Tiffany mixed coal sample at 130°F as predicted by the developed isotherm are shown in Table 21. However, Fig. 14 shows the competitive adsorptions as predicted by the developed isotherm.

Table 20. Laboratory measurement of the competitive adsorption of 50% methane and 50% nitrogen on Tiffany mixed coal sample at 130°F

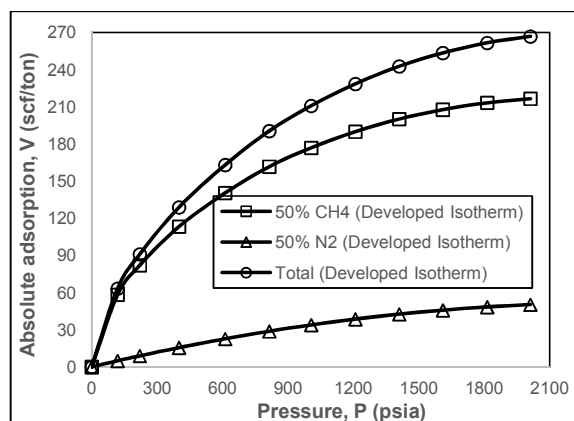| Pressure, P (psia)	$V_{Measured}^{Absolute}$ 50% CH$_4$ (scf/ton)	$V_{Measured}^{Absolute}$ 50% N$_2$ (scf/ton)	$V_{Measured}^{Absolute}$ Total (scf/ton)
118.5	37.1	9.3	46.4
220.1	64.5	16.3	80.8
400.0	100.6	24.1	124.7
611.6	130.9	34.1	165.1
813.9	159.1	36.6	195.7
1005.9	177.1	43.3	220.4
1208.5	196.2	44.5	240.7
1409.7	209.5	49.3	258.7
1609.6	223.8	52.8	276.6
1812.8	231.9	60.6	292.5
2010.8	244.9	66.7	311.6

Source: [34]

Fig. 13. Plot of laboratory adsorption measurement versus pressure for methane and nitrogen competitive adsorption on Tiffany mixed coal sample at 130°F

Table 21. Single-component and competitive adsorption of 50% methane and 50% nitrogen on tiffany mixed coal sample at 130°F as predicted by the developed isotherm
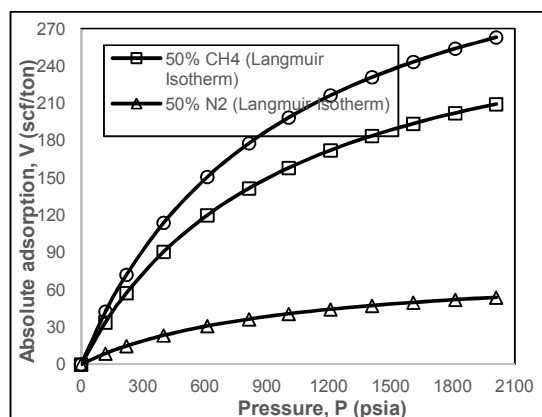
| Pressure, P (psia)	Developed isotherm				
	Single component adsorption		Competitive adsorption		
	$V_{Developed\ Isotherm}^{Absolute}$ 100% CH_4 (scf/ton)	$V_{Developed\ Isotherm}^{Absolute}$ 100% N_2 (scf/ton)	$V_{Developed\ Isotherm}^{Absolute}$ 50% CH_4 (scf/ton)	$V_{Developed\ Isotherm}^{Absolute}$ 50% N_2 (scf/ton)	$V_{Developed\ Isotherm}^{Absolute}$ Total (scf/ton)
118.5	86.73	14.9	58.3	4.9	63.2
220.1	122.0	27.1	82.0	8.9	90.9
400.0	168.5	47.4	113.3	15.5	128.8
611.6	209.5	69.0	140.4	22.6	163.0
813.9	239.9	87.5	161.7	28.7	190.4
1005.9	263.1	103.1	176.9	33.8	210.7
1208.5	282.5	117.5	189.9	38.5	228.4
1409.7	297.6	129.6	200.1	42.5	242.6
1609.6	308.9	139.5	207.7	45.7	253.4
1812.8	317.1	147.4	213.2	48.3	261.5
2010.8	322.1	153.1	216.5	50.2	266.7

Fig. 14. Plot of adsorption versus pressure for methane and nitrogen competitive adsorption on tiffany mixed coal sample at 130°F as predicted by the developed isotherm

Table 22. Adsorption of 50% methane and 50% nitrogen on tiffany mixed coal sample at 130°F as predicted by Langmuir isotherm

Pressure, P (psia)	$V_{Langmuir\ Isotherm}^{Absolute}$ 50% CH_4 (scf/ton)	$V_{Langmuir\ Isotherm}^{Absolute}$ 50% N_2 (scf/ton)	$V_{Langmuir\ Isotherm}^{Absolute}$ Total (scf/ton)
118.5	33.8	8.7	42.5
220.1	57.4	14.7	72.1
400.0	90.6	23.3	113.9
611.6	120.0	30.8	150.8
813.9	141.6	36.3	177.9
1005.9	158.0	40.6	198.6
1208.5	172.2	44.2	216.4
1409.7	183.8	47.2	231.0
1609.6	193.6	49.7	243.3
1812.8	202.1	51.9	254.0
2010.8	209.3	53.7	263.0

Fig. 15. Plot of adsorption versus pressure for methane and nitrogen competitive adsorption on tiffany mixed coal sample at 130°F as predicted by Langmuir isotherm
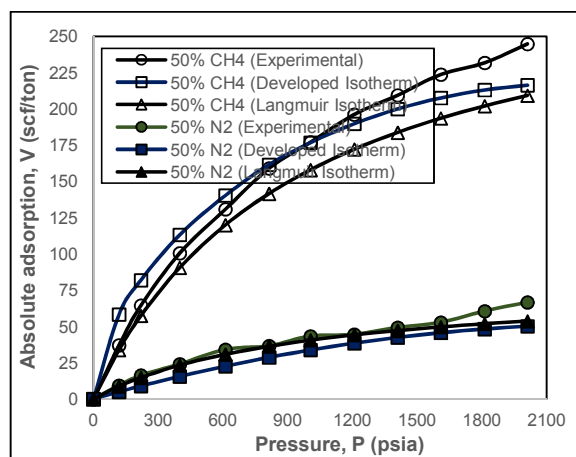
Fig. 16. Correlation and validation of the competitive adsorption of 50% methane and 50% nitrogen on Tiffany mixed coal sample at 130°F

Also, the competitive adsorptions of methane and nitrogen on Tiffany mixed coal sample at 130°F as predicted by Langmuir isotherm are shown in Table 22 while the graphical representation is shown in Fig.15.

The correlation of the competitive adsorption prediction of 50% methane and 50% nitrogen on Tiffany mixed coal sample at 130°F by the developed isotherm and Langmuir isotherm and validation by laboratory measurement are graphically shown in Fig. 16.

The plot (Fig. 16) shows that the developed isotherm prediction of competitive adsorption is better for cases where the adsorbent affinity for the adsorbate is high as displayed in the 50% methane adsorption. However, Langmuir isotherm prediction of competitive adsorption is

better for cases where the adsorbent affinity for the adsorbate is low as displayed in the 50% nitrogen adsorption.

4. CONCLUSION

In this work, a Type-I adsorption isotherm (which assumes a monolayer adsorption like Langmuir isotherm) is developed. The developed isotherm can be used to model all cases of monolayer adsorptions of gases (or fluids) on adsorbents. The developed isotherm discloses and amends the ambiguity surrounding the onset of adsorption saturation pressure in Langmuir isotherm.

The major contributions of the developed isotherm are: (i) offering an effective prediction of low-pressure gas adsorption before the onset of

adsorption saturation pressure (P_s) and showing that maximum adsorbed volume (V_{max}) is maintained constant during pressure increase above the adsorption saturation pressure (P_s), (ii) thus revealing and correcting Langmuir isotherm's over-estimation of adsorbed volume at higher pressures, and (iii) showing that Langmuir isotherm could not actually be referred to as a Type I isotherm but a "*pseudo-Type I*" isotherm.

For gas mixture, Langmuir isotherm prediction of competitive adsorption is found to be better for cases where the adsorbent affinity for the adsorbate is low. However, the developed isotherm prediction of competitive adsorption is observed to be better for cases where the adsorbent affinity for the adsorbate is high.

COMPETING INTERESTS

Authors have declared that no competing interests exist.

REFERENCES

1. Moore WJ. Physical chemistry, prentice-hall, Inc; 1972.
2. Malek A, Farooq S. Comparison of isotherm models for hydrocarbon adsorption on activated carbon. American Institute of Chemical Engineers Journal. 1996;42(11);3191–3201.
3. Langmuir I. The constitution and fundamental properties of solids and liquids. Journal of American Chemical Society. 1916;38(11):2221-2295.
4. Ghiaci M, Abbaspur A, Kia R, Seyedeyn-Azad F. Equilibrium isotherm studies for the sorption of benzene, toluene and phenol onto organo-zeolites and as-synthesized MCM-41. Sep. Purif. Technol. 2004;40:217–229.
5. Kumar KV, Sivanesan S. Sorption isotherm for safranin onto rice husk: Comparison of linear and non-linear methods. Dyes Pigments. 2007;72:130–133.
6. Freundlich HMF. Over the adsorption in solution. J. Phys. Chem. 1906;57:385-471.
7. Markham ED, Benton AF. The adsorption of gas mixtures by silica. J. Am. Chem. Soc. 1931;53:497.
8. Brunauer S, Emmett PH, Teller E. Journal of American Chemical Society. 1938;6: 309.
9. Fowler RH, Guggenheim EA. Statistical thermodynamics. Cambridge University Press, London. 1939;431–450.
10. Temkin MI, Pyzhev V. Kinetics of ammonia synthesis on promoted iron catalyst. Acta Phys. Chim. USSR. 1940;12:327–356.
11. Harkins WD, Jura GJ. Chem. Phys. 1943; 11:430.
12. Sips R. Combined form of langmuir and freundlich equations. J. Chem. Phys. 1948; 16:490–495.
13. Koble RA, Corrigan TE. Adsorption isotherms for pure hydrocarbons. Ind. Eng. Chem. 1952;44: 383–387.
14. Kiselev AV. Vapor adsorption in the formation of adsorbate molecule complexes on the Surface. Kolloid Zhur. 1958;20:338–348.
15. Redlich O, Peterson DL. A useful adsorption isotherm. J. Phys. Chem. 1959; 63:1024–1026.
16. Elovich SY, Larinov OG. Theory of adsorption from solutions of non-electrolytes on solid (I) Equation adsorption from solutions and the analysis of Its simplest form, (II) Verification of the equation of adsorption isotherm from solutions. Izv. Akad. Nauk. SSSR, Otd. Khim. Nauk. 1962; 2:209–216.
17. Myers AL, Prausnitz JM. Thermodynamics of mixed-gas adsorption. AIChE Journal. 1965;11(1): 121-127.
18. Dubinin MM. The potential theory of adsorption of gases and vapors for adsorbents with energetically non-uniform surface. Chem. Rev. 1960;60:235–266.
19. Dubinin MM. Chemistry and physics of carbon in Walker PL, Ed. Marcel Dekker: New York. 1966;2:51-120.
20. Dubinin MM, Astakhov VA. Description of adsorption equilibria of vapors on zeolites over wide ranges of temperature and pressure. Advances in Chemistry Series. 1971;102:69-85.
21. Dubinin MM, Radushkevich LV. The equation of the characteristic curve of the activated charcoal. Proc. Acad. Sci. USSR Phys. Chem. Sect. 1997;55:331–337.
22. Toth J. State equations of the solid gas interface layer, acta chem. Acad. Hung. 1971;69: 311–317.
23. Nitta T, Shigetomi T, Kuro-Oka M, Katayama T. An adsorption isotherm of multi-site occupancy model for homogeneous surface. Journal of Chemical Engineering of Japan. 1984;17(1):39-45
24. IUPAC; 1985.

25. Gregg SJ, Sing KSW. Adsorption, Surface Area and Porosity. London: Academic Press Inc. UK; 1982.

26. Keller J, Staudt R. Gas adsorption equilibria: Experimental methods and adsorption isotherms. Springer Science + Business Media, Inc., Boston; 2005.

27. Merey S. Experimental analysis of adsorption capacities and behaviors of shale samples, M.Sc Thesis, Middle East Technical University, Turkey; 2013.

28. Adekola FA, Adegoke HI, Ajikanle RA. Kinetic and equilibrium studies of Pb(Ii) and Cd(Ii) adsorption on African wild mango (*Irvingia gabonensis*) Shell. Bulletin of the Chemical Society of Ethiopia. 2016;30(2).

29. Chen L, Jiang Z, Liu K, Ji W, Wang P, Gao F, Hu T. Application of langmuir and dubinin–radushkevich models to estimate methane sorption capacity on two shale samples from the upper triassic chang 7 member in the southeastern Ordos Basin, China. Energy Exploration and Exploitation. 2017;35(1);122–144.

30. Jin Q, Huang L, Li A, Shan A. Quantification of the limitation of langmuir model used in adsorption research on sediments via site energy heterogeneity. Chemosphere. 2017;185:518-528.

31. Mahatmanti FW, Rengga WDP, Kusumastuti E. Nuryono. Adsorption of Pb(II) Ion from aqueous solution onto chitosan/silica/polyethylene glycol (Ch/Si/P) composites membrane. IOP Conference Series: Materials Science and Engineering, United Kingdom; 2017.

32. Choy KK, Porter JF, McKay G. Langmuir isotherm models applied to the multicomponent sorption of acid dyes from effluent onto activated carbon. Journal of Chemical Engineering Data. 2018;45(4):575-584.

33. Hamzaoui M, Bestani B, Benderdouche N. The use of linear and nonlinear methods for adsorption isotherm optimization of basic green 4-dye onto sawdust-based activated carbon. Journal of Materials and Environmental Science. 2018;9(4):1110-1118.

34. Gasem KAM, Robinson RL Jr, Reeves SR. Adsorption of pure methane, nitrogen and carbon dioxide and their mixtures on San Juan Basin Coal. DE-FC26-00NT40924 Paper prepared for the U.S. Department of Energy; 2002.

APPENDICES

Appendix A

Derivation of Langmuir Isotherm: Kinetic Approach

Langmuir isotherm describes a progressively increasing surface adsorption as a function of pressure up until the entire surface area is covered with a single layer of molecules and no further adsorption can occur (see Fig. 1).

Considering fluid phase F, vacant surface sites $[S]$, and occupied surface sites $[F_{ads}]$ (number/area); the rates of adsorption and desorption of fluid molecules are R_{ads} and R_{des} respectively.

Rate of adsorption is proportional to the partial pressure P_f of the fluid over the surface and the concentration of vacant sites $[S]$ (number/area):

$$R_{ads} = K_{ads} \cdot P_f \cdot [S] \tag{A.1}$$

where K_{ads} is adsorption rate coefficient.

Rate of desorption is proportional to the concentration of sites filled with fluid molecules $[F_{ads}]$ (number/area):

$$R_{des} = K_{des} \cdot [F_{ads}] \tag{A.2}$$

where K_{des} is desorption rate coefficient.

If adsorption coverage is assumed to be independent of the enthalpy of adsorption, then the dynamic equilibrium parameter K_{eq}^f has a constant value and it is referred to as Langmuir dynamic equilibrium constant.

At dynamic equilibrium, rate of adsorption equals rate of desorption. Hence,

$$K_{eq}^f = \frac{K_{ads}}{K_{des}} = \frac{[F_{ads}]}{P_f \cdot [S]} \tag{A.3}$$

Concentration of all sites $[S_T]$ is the sum of the concentrations of vacant and occupied sites (number/area):

$$[S_T] = [S] + [F_{ads}] \tag{A.4}$$

With reference to (A.3),

$$[S_T] = \frac{[F_{ads}]}{K_{eq}^f \cdot P_f} + [F_{ads}] \tag{A.5}$$

$$[S_T] = [F_{ads}] \left\{ \frac{1 + K_{eq}^f \cdot P_f}{K_{eq}^f \cdot P_f} \right\} \tag{A.6}$$

The fraction of the surface sites occupied by fluid $[F]$ is defined as:

$$\theta = \frac{[F_{ads}]}{[S_T]} \tag{A.7}$$

Hence,

$$\theta = \frac{[F_{ads}]}{[S_T]} = \frac{K_{eq}^f \cdot P_f}{1 + K_{eq}^f \cdot P_f} \tag{A.8}$$

Expressing the partial pressure P_f as P, the occupied surface site $[F_{ads}]$ as the volume of fluid adsorbed V_{ads}, the concentration of all sites $[S_T]$ as the Langmuir volume V_L, (the maximum fluid adsorbable), and the Langmuir dynamic equilibrium constant K_{eq}^f as b; the fractional loading of the surface sites is then expressed as:

$$\theta = \frac{V_{ads}}{V_L} = \frac{bP}{1+bP} \tag{A.9}$$

$$V_{ads} = V_L \cdot \frac{bP}{1+bP} \tag{A.10}$$

Equation (A.10) is the Langmuir adsorption isotherm where b is the Langmuir dynamic equilibrium constant determined as $\frac{1}{P_L}$ and P_L is the Langmuir pressure (the pressure at a volume $\frac{V_L}{2}$). Therefore, Langmuir isotherm could be expressed as:

$$V_{ads} = V_L \cdot \frac{P}{P+P_L} \tag{A.11}$$

Appendix B

Derivation of Pressure P_β and Adsorbed Volume V_β at Inflexion Point β where $\Delta\left(\frac{V}{V_{max}}\right) = \Delta\left(\frac{P}{P_s}\right)$ on the Developed Isotherm

With reference to Equation 14,

$$\frac{dP_a}{dP} = \frac{d}{dP}\left\{(P_s - P)\left(\frac{P}{P_s}\right)^n\right\} \tag{B.1}$$

$$\frac{dP_a}{dP} = \frac{d}{dP}\left\{\left(\frac{P_s}{P_s^n}\right)P^n - \left(\frac{1}{P_s^n}\right)P^{n+1}\right\} \tag{B.2}$$

$$\frac{dP_a}{dP} = n\left(\frac{P_s}{P_s^n}\right)P^{n-1} - (n+1)\left(\frac{1}{P_s^n}\right)P^n \tag{B.3}$$

However, $\frac{dP_a}{dP} = 0$ at inflexion point β where $\Delta\left(\frac{V}{V_{max}}\right) = \Delta\left(\frac{P}{P_s}\right)$ on the developed isotherm. Hence, at pressure P_β,

$$n\left(\frac{P_\beta^n}{P_s^n}\right)\left(\frac{P_s}{P_\beta}\right) = (n+1)\left(\frac{P_\beta^n}{P_s^n}\right) \tag{B.4}$$

$$n\left(\frac{P_s}{P_\beta}\right) = (n+1) \tag{B.5}$$

$$P_\beta = \left(\frac{n}{n+1}\right)P_s \tag{B.6}$$

and

$$V_\beta = V_{max}\left\{\frac{P_\beta}{P_s} + \left(1 - \frac{P_\beta}{P_s}\right)\left(\frac{P_\beta}{P_s}\right)^n\right\} \tag{B.7}$$